Virtual and Physical Prototyping, 2014
http://dx.doi.org/10.1080/17452759.2014.984042

Taylor & Francis
Taylor & Francis Group

Thermal conditions affecting heat transfer in FDM/FFE: a contribution towards the numerical modelling of the process

S.F. Costa, F.M. Duarte, and J.A. Covas*

I3N/IPC - Institute for Polymers and Composites, Department of Polymer Engineering University of Minho, Guimarães, Portugal

(*Received 9 September 2014; accepted 31 October 2014*)

The performance of parts produced by Free Form Extrusion (FFE), an increasingly popular additive manufacturing technique, depends mainly on their dimensional accuracy, surface quality and mechanical performance. These attributes are strongly influenced by the evolution of the filament temperature and deformation during deposition and solidification. Consequently, the availability of adequate process modelling software would offer a powerful tool to support efficient process set-up and optimisation. This work examines the contribution to the overall heat transfer of various thermal phenomena developing during the manufacturing sequence, including convection and radiation with the environment, conduction with support and between adjacent filaments, radiation between adjacent filaments and convection with entrapped air. The magnitude of the mechanical deformation is also studied. Once this exercise is completed, it is possible to select the material properties, process variables and thermal phenomena that should be taken in for effective numerical modelling of FFE.

Keywords: computer-aided engineering; free-form; fused deposition modelling (FDM)

1. Introduction

Additive Manufacturing (AM) is defined as '*the process of joining materials to make objects from 3D model data, usually layer upon layer, as opposed to subtractive manufacturing methodologies, such as traditional machining*' (ASTM Standard 2012). Over the past two decades, and particularly in the last few years, tremendous improvements in technology and materials, coupled to advances in modelling and design, resulted in many successful applications, ranging from simple designs or prototypes to geometrically intricate parts (Chua and Leong 2014, Mellor *et al*. 2014, Sugavaneswaran and Arumaikkannu 2014). The industrial and societal awareness already attained by these techniques will certainly guarantee a spectacular growth in the near future (Brookes 2014). For example, three-dimensional (3D) printing has been included in the list of the most '*disruptive technologies*', i.e., with annual growth rates above 20% (Goldman Sachs 2013).

Fused deposition modelling (FDM) (also denoted as Fused Filament Fabrication (FFF)) is presently one of the most popular AM techniques due to its easy operation, utilisation of environmentally safe materials and reproducibility (Boschetto *et al.* 2013). It uses a nozzle tip [eventually with a customised design (Choia *et al*. 2011)] fed by a polymer rod to generate a thin melted filament that is deposited onto successive part layers. Given its simplicity in terms of sequence and control, equipment is being offered at increasingly lower cost (Brookes 2014). In parallel, polymers are supplied as re-fills, spools or cartridges, even if only a few types are commercially available. Free Form Extrusion (FFE) is a variant of FDM where the filament is created by an extruder and die assembly (Bellini 2002, Reddy *et al*. 2007, Lee *et al*. 2014, Silveira *et al*., 2014). This widens the range of accessible materials (e.g. most polymers and copolymers, polymer blends, filled and reinforced polymers, thermoplastic vulcanisates, nanocomposites, etc.), thus creating new possibilities in terms of part performance and attributes (David *et al*. 2014, Espalin *et al.* 2014). Additionally, the implementation of co-extrusion, or sequential extrusion techniques, would extend the process potential by

*Corresponding author. Email: jcovas@dep.uminho.pt

combining different materials in a single part, e.g. soft/hard, compact/foamed or electrically conductive/insulating zones, as well as transparent/opaque/multicolour effects. For example, FFE was used to fabricate poly-ε-caprolactone (PCL) tissue scaffolds (Wang *et al*. 2004) and to create ceramic parts (Bellini *et al.* 2005, Leu *et al*. 2012).

Successful and widespread utilisation of FDM/FFE requires the capacity to generate products with satisfactory dimensional accuracy, surface quality and mechanical performance. These properties are determined by the filament deformation during deposition and solidification and by the quality of the bonding between contiguous filaments (Céline *et al.* 2004, Cunico 2013, Martínez *et al*. 2013). Each filament should solidify as quickly as possible to avoid excessive deformation due to gravity (and, in some situations, also due to the weight of the material deposited above it) but, simultaneously, adequate bonding requires that neighbouring filaments should remain sufficiently hot for enough time. These seem conflicting prerequisites. Modern 3D printers have cooling fans near to the nozzle tip, but their control is usually very limited.

The effect of various process variables on the properties of FDM parts were investigated, extrusion temperature and/or deposition rate being identified as the major parameters influencing bonding (Pandey *et al*. 2006, Pal and Ravi 2007, Galantucci *et al.* 2009, Widden and Gunn 2010, Syam *et al.* 2011, Boschetto *et al.* 2013, Croccolo *et al*. 2013, Cunico 2013, Rezaie *et al*. 2013, Gurrala and Regalla 2014b). However, for process set-up and optimisation purposes, it is also essential to know the evolution of the filament temperature during deposition and how it is affected by all operator-dependent variables, such as extrusion temperature and production rate, environment temperature (e.g. use of a heating chamber vs. direct deposition onto a free heated support), filament cross-section and deposition sequence. Yardimci and Güçeri (1996) and Li (2002) studied transient convective heat transfer on a single filament element. Rodriguez (1999) used the ABAQUS® software to compute the temperature profile in an elliptical filament and developed a 2D analytical solution for a rectangular filament. Temperatures in a cross-section were calculated assuming convection with the environment but with distinct initial temperatures, depending on the existence of contact with another filament. These analyses ignore the existence of contacts and/or assume perfect contact between filaments. Also, they are only applicable to a specific cross-section and not to the entire product volume. As for the filaments deformation, a few experimental studies (e.g. Ziemian and Crawn 2001, Pennington *et al*. 2005, Gurrala and Regalla 2014a) revealed that part size, part location in the chamber and environment temperature have a significant effect on dimensional accuracy.

Given the over simplicity of previous thermal analyses, the present work examines the contribution to heat transfer in FDM/FFE of most process variables and thermal phenomena, such as convection and radiation with the environment, conduction with support and between adjacent filaments, radiation between adjacent filaments and convection with entrapped air. The magnitude and related influence on heat transfer of the mechanical deformation of filaments (due to changes in the contact area) within the practical range of deposition temperatures is also studied. The results enabled the identification of the material properties, process variables and thermal phenomena that should be included for effective modelling of FDM/FFE.

2. Modelling heat transfer and mechanical deformation in FDM/FFE

2.1 Heat transfer

When the first filament (or filament segment) of the bottom layer of the part is deposited onto the support, heat exchanges by convection and radiation develop with the surroundings and by conduction with the support. As the remaining filaments (or filament segments) of this first layer are laid, new physical contacts are created and heat exchanges by conduction between adjacent filaments must be considered. Upon the deposition of new layers, new physical contacts are generated; hence, several heat transfer modes change and heat transfer with air entrapped between contiguous filaments may also develop. The order of incidence of the contacts and their features (shape and area) are dictated by the deposition strategy. It has been experimentally demonstrated that the latter strongly influence both the final mechanical properties (Bellini and Güçeri 2003) and surface finish (Thrimurthulu *et al*. 2004).

As illustrated in the flowchart of Figure 1, this heat transfer problem can be tackled assuming the movement at constant rate of a filament with uniform cross-section, small axial increments of which are deposited at Δt intervals, according to a pre-established sequence. At each elementary time step:

(1) the relevant boundary conditions of every increment are updated according to local conditions;
(2) the temperature evolution of the newest filament increment (considered as a mesh of quadratic elements), as well as that of all the previously deposited ones (due to the effect of new contacts), is calculated;
(3) estimating the differences in temperature of nodes at the centre and opposing edges of a given cross-section, the existence of a 'thermally thin' filament (i.e. with uniform temperature at each cross-section) is assessed; similarly, one can ascertain whether longitudinal heat transfer is meaningful by computing the temperature evolution of two sequential elements deposited at instants t and $t+\Delta t$, for two distinct conditions at their interface: no contact and perfect contact. The initial temperature of the last deposited element is the extrusion temperature, while the temperature of the previously deposited element is the

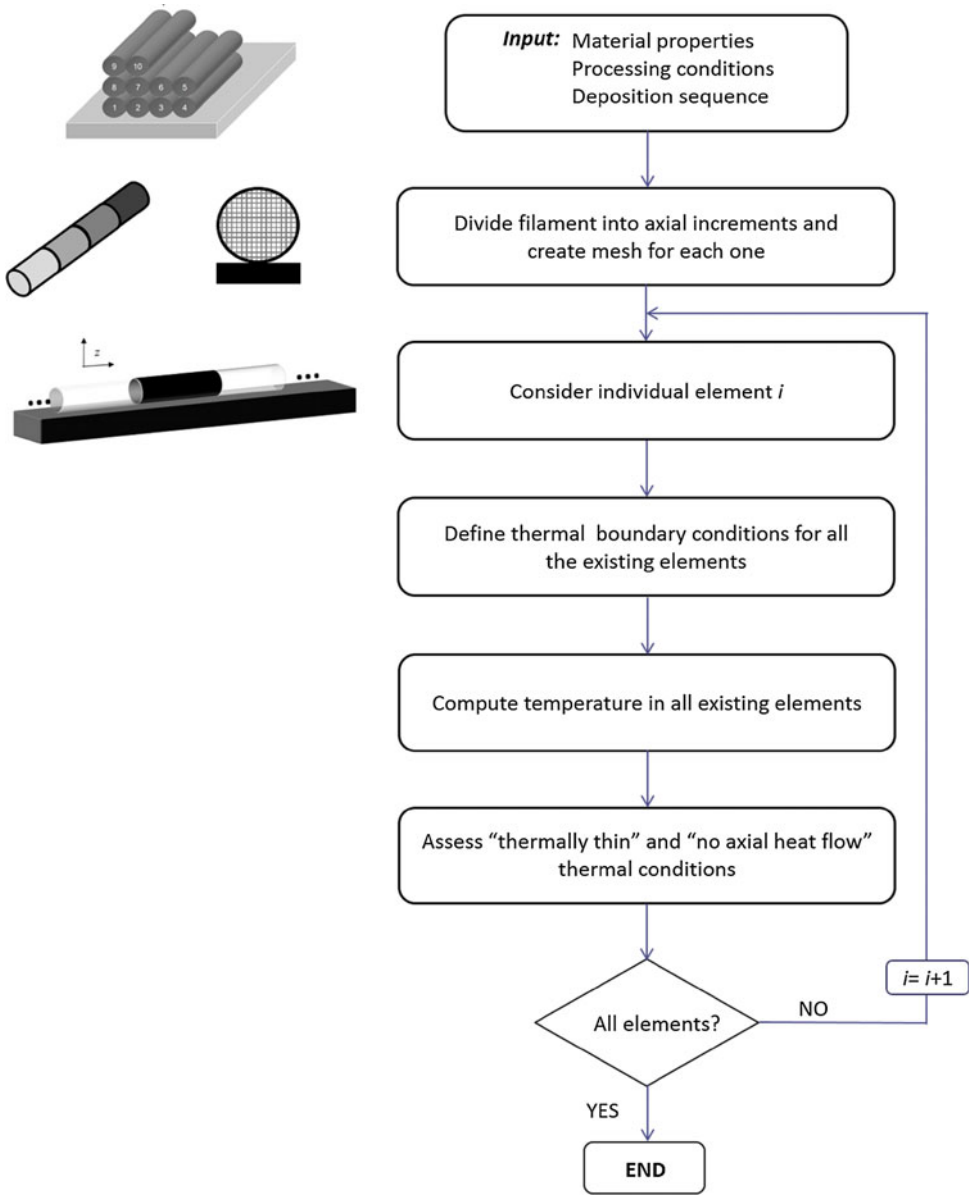

Figure 1. Procedure to compute heat transfer evolution for a given deposition configuration.

temperature after cooling for Δt seconds. If the temperature evolution of the two elements is identical for the two boundary conditions, the longitudinal heat flux is negligible.

Each axial filament increment consisted of a regular mesh of 262 quadratic elements per cross-section and 20 along the axis and was created by extruding for 0.1 s. The interfacial contact area between filaments and between filaments and support is 5% of their surface area. Tables 1 and 2 present the operating conditions assumed in the calculations and the ABAQUS® parameters selected, respectively. The former are typical for FDM, for example using a Stratasys 1600 FDM machine (Rodriguez *et al*. 2000). As for the ABAQUS® parameters, the selected number of elements provided a good compromise between computing time and accuracy. The Newton's method is typically adopted to solve non-linear equilibrium equations, whilst the element type and integration mode are adequate for the solution technique utilised.

Table 1. Operating conditions of FDM/FFE.

Property	Value
Extrusion temperature, T(ºC)	270
Environment temperature, T_E (ºC)	70
Extrusion velocity (m/s)	0.025
Filament diameter (m)	0.0003

Table 2. ABAQUS® parameters used for the heat transfer simulations.

Property	Value
Number of quadratic elements	5240
Element type	DC3D8: 8-node linear heat transfer brick
Incremental time	10^{-12} s – 0.1 s
Solution technique	Full Newton
Default load variation with time	Instantaneous
Output request	NT, Nodal Temperature

The thermal conditions were activated instantaneously (default load variation with time).

2.2 Mechanical deformation

The ABAQUS® software was also used to compute the deformation of a filament subjected to its own weight, as well as to the weight of a vertical stack of similar filaments on top. Calculations were performed assuming either purely elastic behaviour, or a viscoelastic response described by a Prony series fit to experimental data (Drabousky 2009). Prony series is a finite series of exponential decay elements that represent the time-dependent shear modulus $G(t)$ as (Brinson and Brinson 2008):

$$G(t)/G_0 = 1 - \sum_{i=1}^{n_p} g_i\left(1 - e^{\frac{-t}{\tau_i}}\right) \quad (1)$$

where $G_0 = G(0)$ is the initial shear modulus (Pa), n_p is the number of Prony terms, g_i is the i^{th} Prony constant, τ_i is the i^{th} Prony retardation time constant and $\sum_{i=1}^{n_p} g_i \leq 1$. The calculations (see Figure 2) were performed at various constant temperatures. Table 3 displays the ABAQUS® parameters utilised. Pressure is applied linearly over the step, given the gradual deposition of the filaments.

3. Material

The model developed is general and can be applied to any thermoplastic polymer system as long as the corresponding thermo-physical properties are available. Although different polymers [e.g. Poly(lactic acid) (PLA) and Acrylonitrile Butadene Styrene Terpolymer (ABS)] may have quite distinct properties at room temperature, successful deposition requires similar thermal, mechanical and rheological properties, which are achieved by proper choice of the operating conditions.

ABS was selected as a case study, given its widespread utilisation. Data in Table 4 corresponds to that of material (ABS-P400, Stratasys Inc.) commonly used in FDM (Rodriguez 2000, Ahn *et al*. 2002). Table 5 shows the Prony series constants at different temperatures, which were computed from $G(t)$ data available in the literature (Vogtmann 2009) (with a Poisson coefficient of 0.4). Fitting to the data can be seen in Figure 3.

4. Results and discussion

4.1 Convection with the environment

Convective heat exchanges with the environment have been considered in all previous FDM/FFE models through the usage of a heat transfer coefficient, h_{conv}. Rodriguez *et al*. (2000) adopted the Churchill correlation for natural convection to estimate h_{conv} = 67 W/m^2·ºC for an elliptical filament (semi-axes of 0.508 mm and 0.254 mm) extruded at 270ºC towards an environment at 70ºC.

Figure 4a shows the temperature evolution during 15 s of cooling of a single circular filament considering exclusively heat exchanges by convection with the environment, for h_{conv} = 5, 60 and 150 W/m^2·ºC. As anticipated, the effect of this coefficient is significant, particularly in the initial cooling instants. This can be clearly seen in Figure 4b, which represents the time necessary for the filament to reach its glass transition temperature, T_g, or the environment (oven) temperature, T_E. As h_{conv} is increased from 5 to 60 W/m^2·ºC, the cooling time needed to reach T_g decreases from 66 to 3 seconds (22 times); a further increase to 150 W/m^2·ºC brings about a reduction of merely 2 times.

4.2 Radiation with the environment

Radiative heat exchanges between the filament and the surroundings were mentioned by Yardimci (1999), but apparently neglected in previous computations. Figure 5 depicts the filament temperature profiles considering heat flux by convection, radiation (emissivity coefficient ε = 0.96) and both together, for the same three values of h_{conv} taken in Figure 4a (5, 60 and 150 W/m^2·ºC). The dependence is non-linear, although the curvature is small. The results show that radiation can be predominant over convection when h_{conv} is small. In this case, calculations assuming convection, or convection and radiation, will yield filament temperature differences after cooling for 15 seconds of up to 10ºC. However, for values of h_{conv} around and above 60 W/m^2·ºC, which should correspond to most practical conditions, filament cooling becomes convection controlled.

4.3 Conduction with support

As the extruded filament contacts the cooler support, heat transfer by conduction between both develops. Due to the thermal contact resistance, r_c, a temperature difference arises at the interface (Kothandaraman and Subramanyan 2006). The value of r_c (m^2 · ºC/W) is governed by surface roughness,

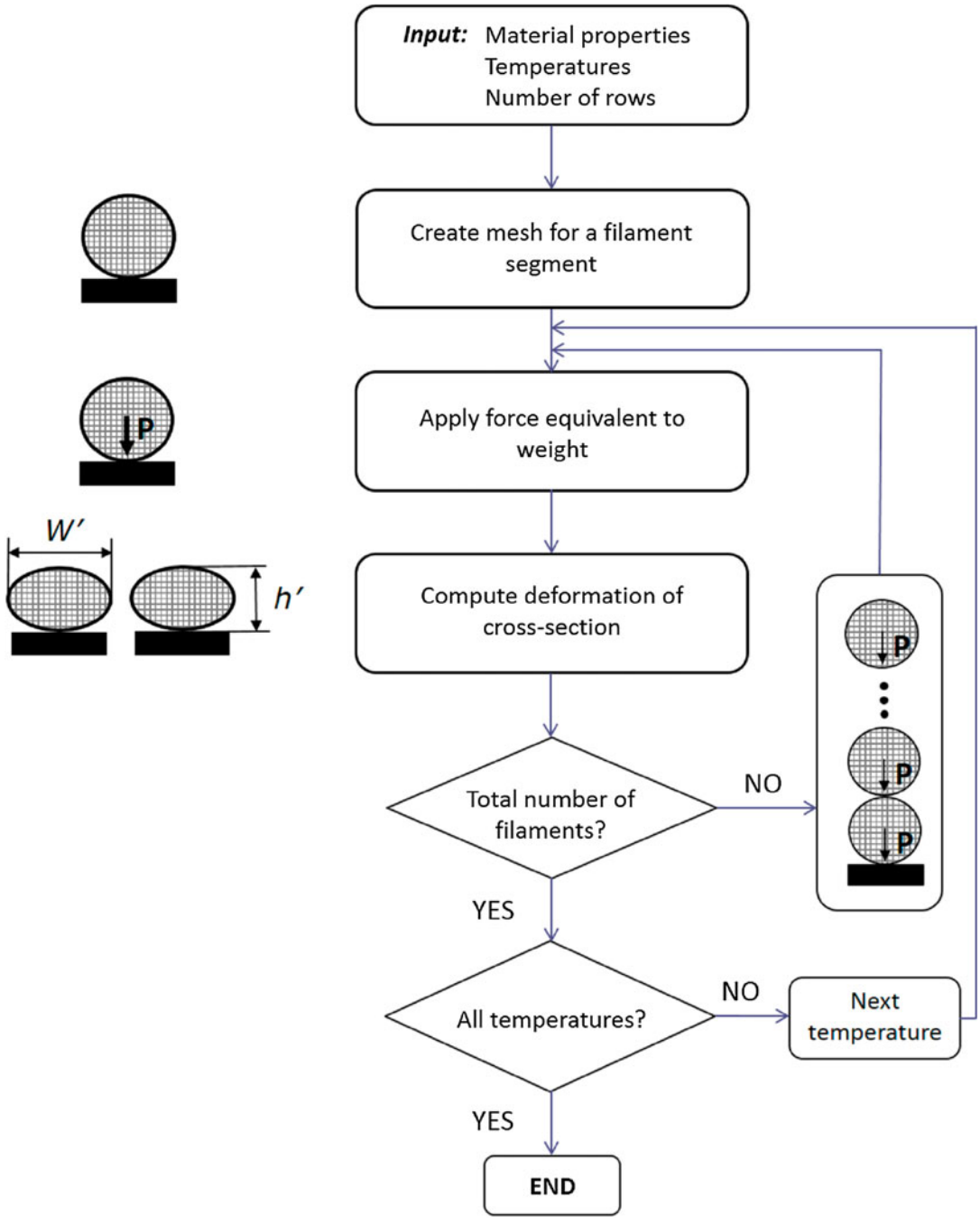

Figure 2. Procedure to compute the mechanical deformation of a vertical pile of filaments.

hardness of the materials, applied pressure and temperature (Kaviany 2002). The thermal contact conductance, h_c (W/m^2·ºC) and r_c are related by:

$$h_c = \frac{1}{A_a r_c} \tag{2}$$

where A_a is the contacting area (m^2). The ABAQUS® software computes h_c according to the value attributed to the '*gap conductance*', which defines the degree of conduction between two bodies. Small values of '*gap conductance*' (10 W/m^2·ºC) correspond to low heat transfer by conduction, and vice-versa.

Figure 6 shows the temperature evolution of cylindrical and parallelepiped (square cross-section) filaments, for low and high gap conductances (10 and 500 W/m^2·ºC, respectively), while h_{conv} was set at 60 W/m^2·ºC. In the case of a circular filament, the contact with the support is minimal (5% of the

Table 3. ABAQUS® parameters used for the deformation simulations.

Property	Value
Number of Elements	4832
Mesh Type	Wedge
Element Type	C3D8R: 8-node linear brick, reduced integration, hourglass control.
Step Type	Simulation 1: Static General Simulation 2: Visco
Increment Size	Initial = 10^{-25} s 10^{-50} s – 0.5 s
Solution technique	Full Newton
Default Load Variation with Time	Ramp linearly over step
Output Request	U, Displacement

Table 4. Properties of ABS-P400 (Rodriguez 2000).

Property	Value
Tensile Strength (MPa)	37
Tensile Modulus (MPa)	2320
Yield strain (%)	3
Glass Transition Temperature (T_g) (ºC)	108
Heat Deflection temperature (HDT) (ºC)	96
Thermal conductivity (W/m ºC)	0.18
Specific heat (J/kg ºC)	2020
Density (kg/m^3)	1050

Table 5. Constants of the Prony series.

@ 95 ºC		@ 110 ºC		@ 135 ºC	
τ_i	g_i	τ_i	g_i	τ_i	g_i
0.1	0.01	0.1	0.01	0.1	0.01
1	0.34	1	0.35	1	0.01
7	0.33	7	0.24	5	0.15
100	0.13	100	0.21	100	0.52

surface area), therefore the heat exchange is small. However, for square filaments, the area in contact attains 25% of the total surface; hence, cooling of the filament is significantly faster. Consequently, heat exchange with the support is controlled both by the thermal contact conductance and contact area.

4.4 Conduction between adjacent filaments

To estimate the contribution of heat conduction between adjacent filaments, a simple deposition sequence must be implemented. As illustrated in Figure 7, two filaments were laid onto the support and parallel to each other, followed by two other filaments on top of them (see inset in Figure 7, where the numbers 1 to 4 define the deposition sequence). The operation lasted 4 seconds (1 second per filament). Each of the graphs in Figure 7 presents the temperature evolution at the centre of each of these four filaments. Three distinct thermal conditions between filaments were assumed: i) no conduction ('*gap conductance*' = 0 W/m^2·ºC); ii) low conduction ('*gap conductance*' = 100 W/m^2·ºC); iii) perfect conductance, with good adhesion between filaments ('*gap conductance*' = 10^6 W/m^2·ºC). The '*gap conductance*' between filament(s) and support was taken as 10 W/m^2·ºC.

Figure 7 confirms that when conduction is nil, there is no mutual thermal interference. The curves are shifted horizontally, because each filament starts cooling down with a delay of one second relative to the preceding one. When conduction exists, the '*gap conductance*' and deposition sequence determine the intensity of the interactions, hence the observed shape of the curves and the differences in temperature in each section. When filaments deposited at different times become in contact, the temperature of the cooler one increases due to the heating caused by the warmer one, the temperature variation being larger the higher the temperature difference between both. In the present case study, when filament 4 contacts filament 1, the temperature of the latter rises approximately 8°C (from 158.1 to 165.6ºC). However, if a node at the top surface had been considered, the temperature increase would have reached 25°C (from 167.8 to 192.8ºC). Conversely, the temperature of filament 4 decreases very rapidly from 270ºC (extrusion temperature) to 230°C. As expected, the magnitude of these phenomena increases with conduction efficiency.

4.5 Radiation between adjacent filaments

When filaments have a circular or elliptic cross-section, their surface will only partially contact that of neighbouring filaments in the same or nearby layers (a certain distance between contiguous filaments may also be pre-set, in order to produce lighter parts). Since filaments are deposited sequentially and start cooling at different times, the exposed (non-contact) area of each filament can exchange radiant heat with the neighbouring ones. This is controlled by a 'view factor' (also known as shape factor) that represents the ratio of radiation energy leaving one surface that is intercepted by another surface. It was calculated for configurations consisting of either parallel or perpendicular identical surfaces and assuming that the exposed surfaces of the filaments were planar (Siegel and Howell 1992).

The same sequence of four filaments depicted in Figure 7 was studied, now for a gap conductance between filament(s) and support of 10 W/m^2·ºC and for a heat transfer coefficient of 60 W/m^2·ºC. Differences in filament temperature allowing for or ignoring radiation were lower than 0.3ºC, i.e. they have a minor impact on heat transfer in FDM/FFE.

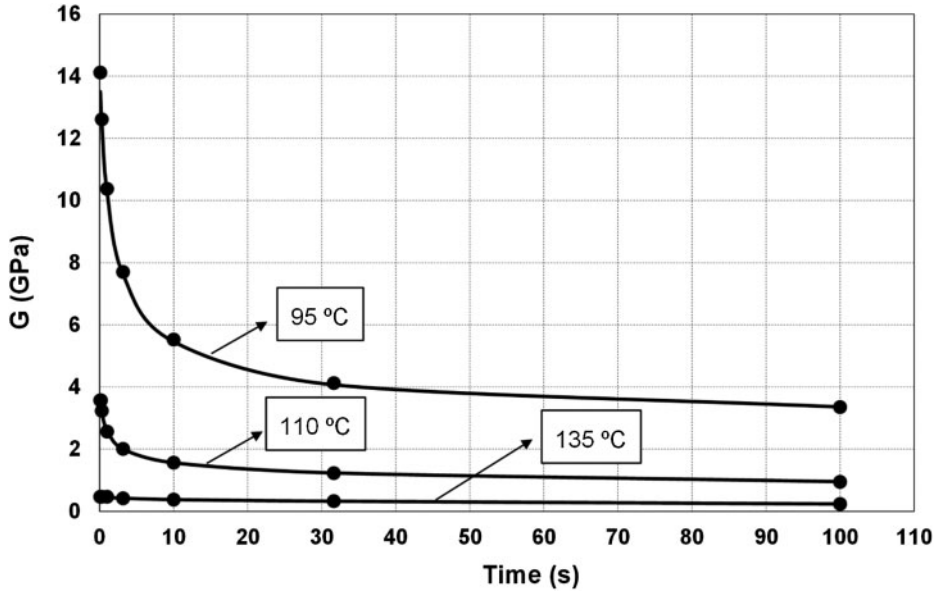

Figure 3. Fitting of experimental $G(t)$ data (•) with a Prony series (solid lines) for the material used in the thermal studies.

4.6 Convection with entrapped air

As argued above, the surface of deposited filaments may touch only partially that of neighbouring filaments in the same or nearby layers. As illustrated in the inset of Figure 7, small pockets of entrapped air may be formed, their temperature being higher than that of the environment.

In order to estimate the relevance of this contribution to the global heat transfer, the same deposition of four filaments was studied. The free volume was considered as a continuous medium with the properties of air at 70ºC (conductivity of 0.03 W/m·ºC, density of 0.998 kg·m^3 and a specific heat of 1009 J/kg·ºC). Even when varying the air temperature between 70 and 180ºC, the influence of the heat exchanges by convection with the entrapped air never caused temperature variations in the filaments larger than 1.1ºC.

4.7 Mechanical deformation of the filaments

This section aims at estimating the order of magnitude of the mechanical deformation of a part obtained by FDM/FFE, with the aim of determining whether the phenomenon should be taken into consideration during process modelling. Thus, it makes sense to select conditions promoting deformation, i.e., a tall part and a small deposition rate. A column of 200 filaments (reaching a height of 60 mm), deposited on top of each other every 0.5 second, was taken as a case study.

Isothermal loadings at 95ºC, 110ºC and 135ºC for both elastic and viscoelastic material responses were studied. Real deformations should be lower, as deposition is strongly non-isothermal, with the 'older' filaments progressively gaining higher resistance to deformation. Figure 8 presents the predicted vertical and horizontal deformations of the most deformed filament, the one at the bottom of the pile. The overall response is non-linear, although with a small curve at these magnitudes. As expected, even for an elastic response deformation increases with time and temperature, since more material is loaded on top of the filament and the modulus decreases, respectively. Although viscoelastic characteristics will obviously induce higher deformations, the total values attained are rather small, less than 0.5% vertically and 0.3% horizontally, at 135ºC.

Table 6 presents the total vertical deformation of the pile of 200 filaments. Since the evolution of the deformation of each individual filament is known (data equivalent to that exhibited in Figure 8), the total value can be determined adding each individual deformation. The global deformations are obviously much smaller than those attained by the filament at the bottom. The results clearly show that – in the range of temperatures studied – the mechanical deformation of the filaments is negligible and should not affect the dimensional accuracy of the part, nor the thermal exchanges (by virtue of variations in surface area).

5. Conclusions

FFE/FDM is growing steadily in importance to manufacture, in a simple way, prototypes or real products well suited to automotive, defence, medical, aerospace and consumer applications. This work used the ABAQUS® software to examine the contribution to the overall heat transfer of various thermal

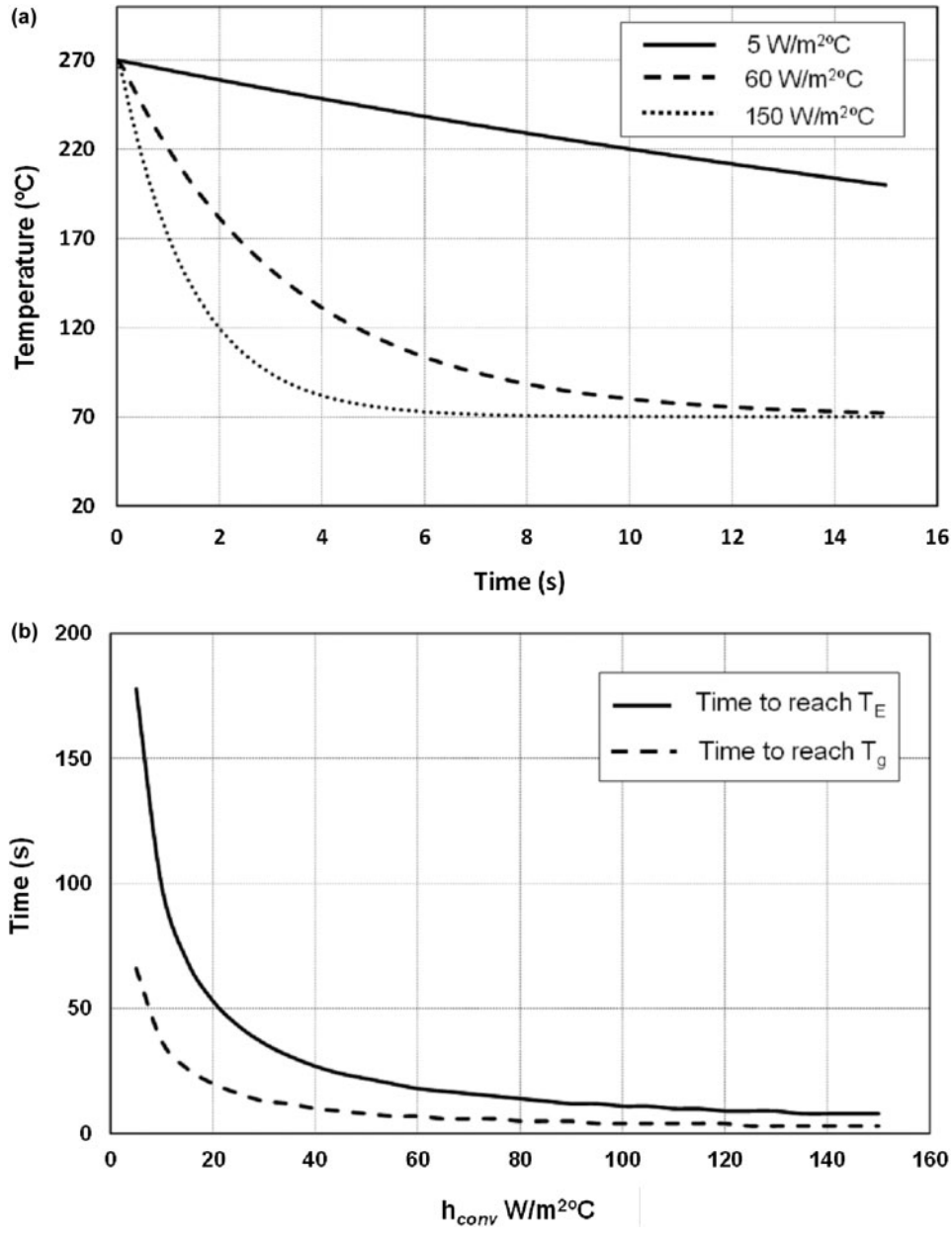

Figure 4. Effect of h_{conv} on filament cooling; a) temperature evolution for h_{conv} = 5, 60 and 150 W/m^2·ºC. b) cooling time needed to reach T_g *or* T_E for various h_{conv}.

phenomena developing during manufacture of a part. The simultaneous mechanical deformation of the assemblage was also studied.

Heat exchanges by convection with the environment and by conduction between adjacent filaments and machine support have the highest impact. The significance of the heat exchanges by radiation with the environment depends on the magnitude of the heat transfer coefficient. When h_{conv} reaches 60 W/m^2·ºC, they can be neglected. Conversely, heat exchanges by radiation between adjacent filaments and by convection with air pockets can be ignored in practice. Temperatures across any filament cross-section are relatively uniform, except when thermal contacts are perfect; also, the higher the degree of conduction, the lower the temperature

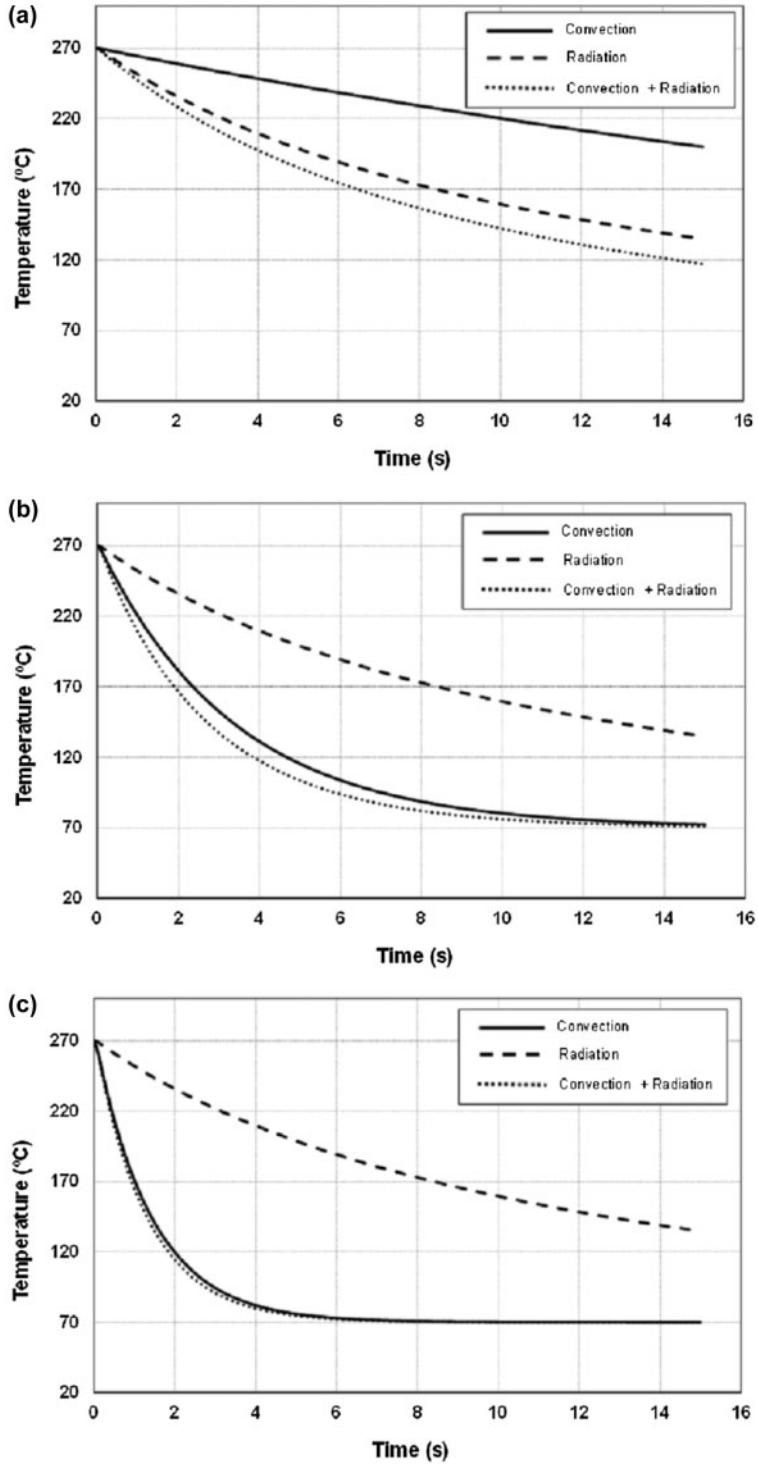

Figure 5. Effect of cooling mode (convection, radiation, both together) on filament cooling; a) h_{conv} = 5 W/m^2·ºC; b) h_{conv} = 60 W/m^2·ºC and c) h_{conv} = 150 W/m^2·ºC.

uniformity. Likewise, temperatures along small filament length increments are uniform, that is, axial conduction can be neglected.

The total mechanical deformation of the filaments due to their own weight is very small and, consequently, its influence on heat transfer and dimensional accuracy of the part is

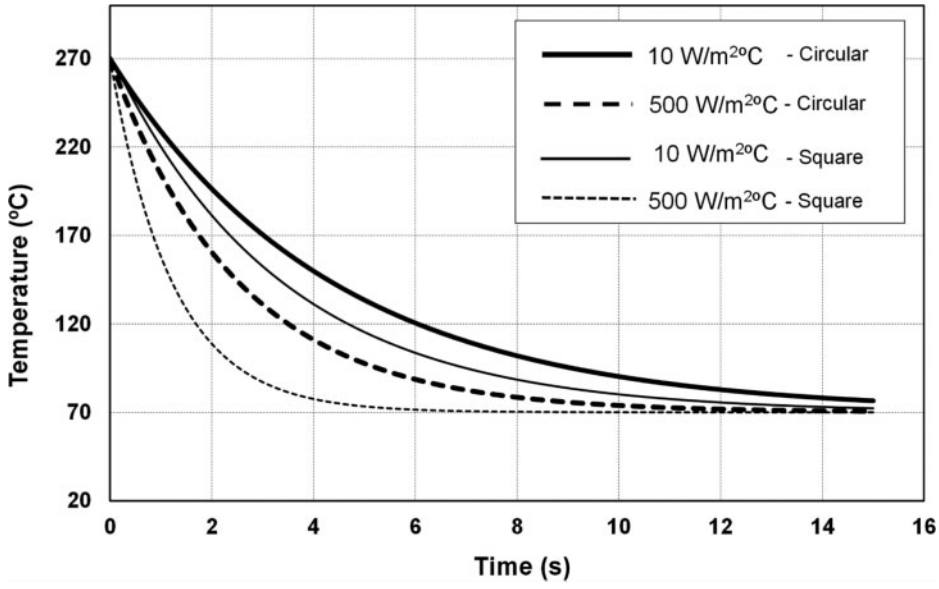

Figure 6. Temperature evolution of filaments with circular and square cross-sections, for low and high gap conductance.

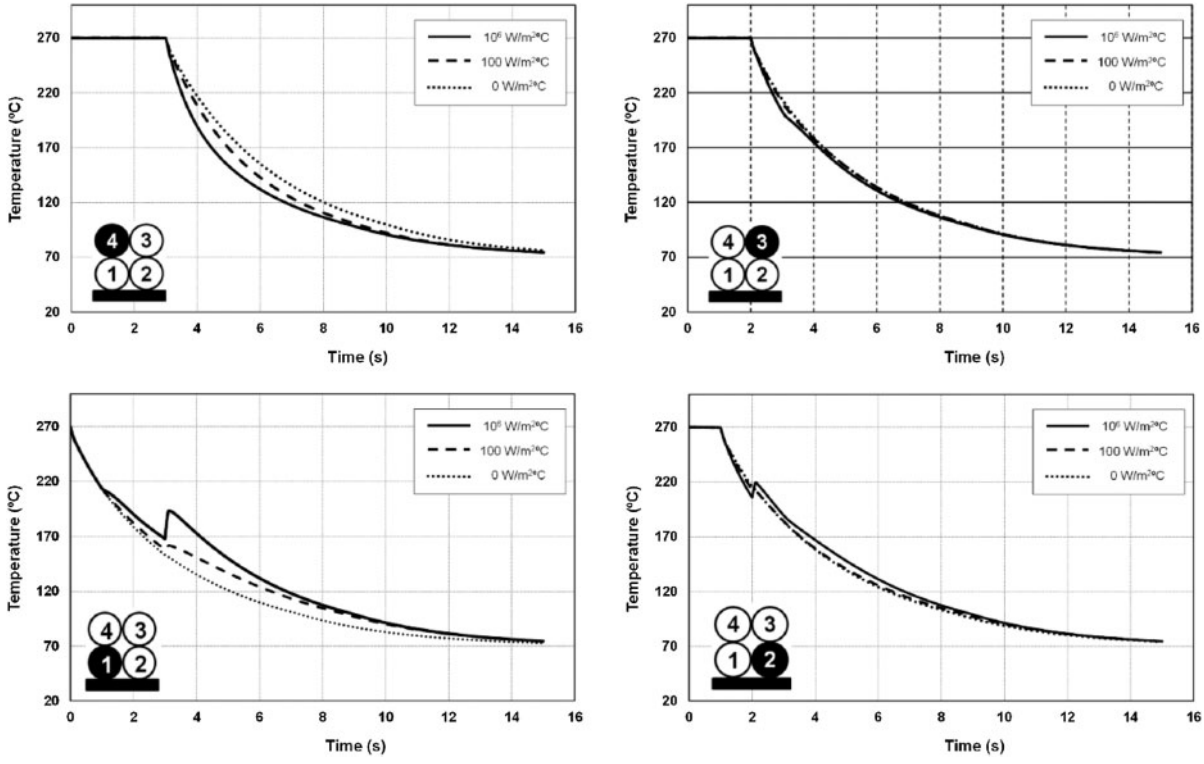

Figure 7. Temperature evolution (at the central node) of four filaments deposited sequentially, considering different thermal conditions at the surface.

insignificant. Although only a limited number of case studies were discussed, the conclusions can be generalised.

The next step will consist of applying the process modelling software (using the initial and boundary thermal conditions selected above) to the deposition of pertinent parts. If the latter comprise more than one material, the correct physical-thermal properties should be applied depending on the local material structure.

Table 6. Total vertical deformation after deposition of a column of 200 filaments with an initial height of 60 mm (elastic and viscoelastic responses).

		Temperature		
		95ºC	**110ºC**	**135ºC**
Elastic behaviour	Total height (mm)	59.998	59.993	59.952
	Total deformation (%)	0.000	0.001	0.080
Viscoelastic behaviour	Total height (mm)	59.993	59.972	59.867
	Total deformation (%)	0.012	0.047	0.222

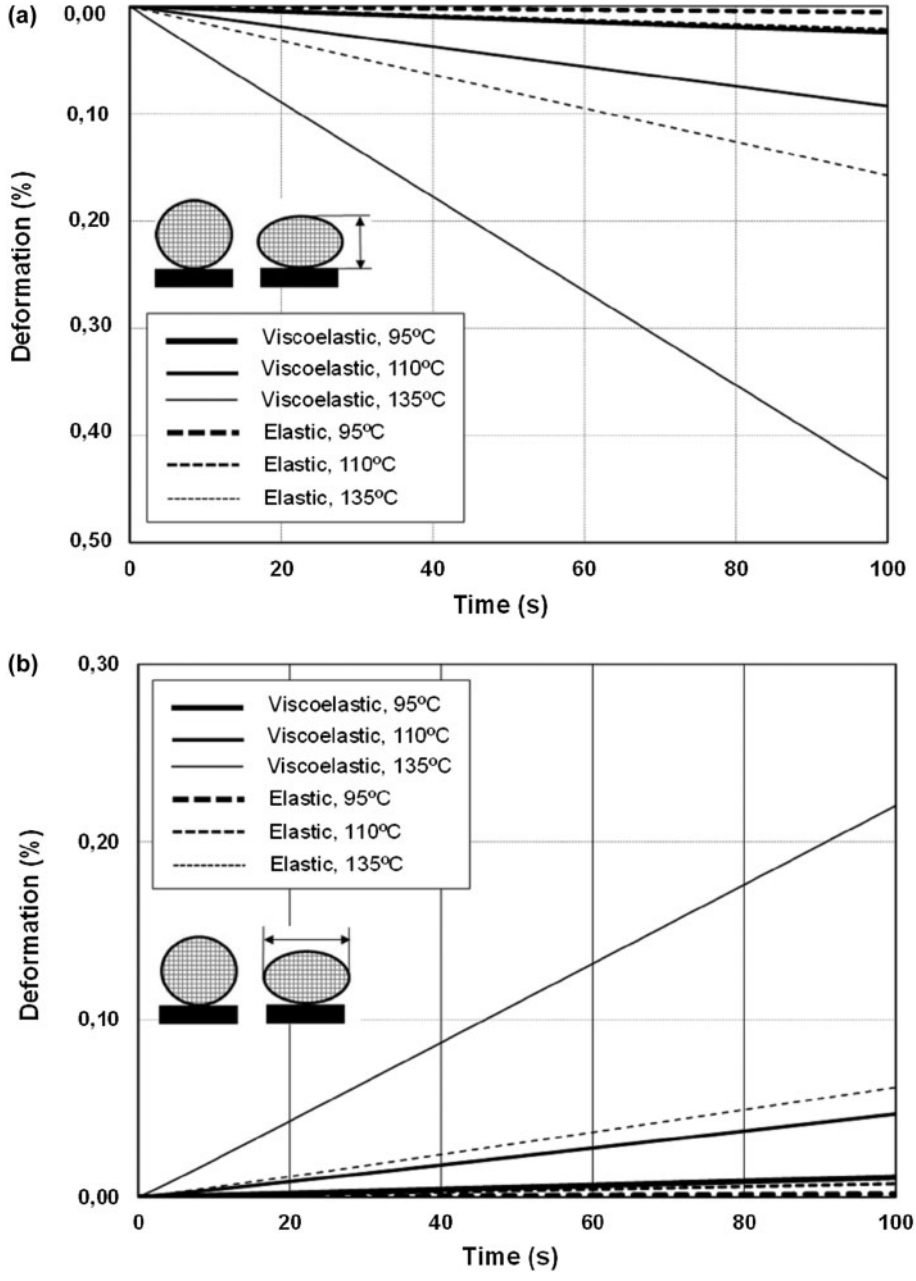

Figure 8. Deformation (in percentage of the original diameter) of a circular filament subjected to the weight of 199 filaments deposited on top, assuming elastic and viscoelastic responses; a) vertical direction; b) horizontal direction.

Disclosure statement

No potential conflict of interest was reported by the authors.

Funding

This work was supported by Strategic Project - LA 25 - 2013–2014 [PEst-C/CTM/LA0025/2013].

References

Ahn, S., *et al*., 2002. Anisotropic material properties of fused deposition modelling ABS. *Rapid Prototyping Journal*, 8 (4), 248–257.

ASTM Standard, F2792 – 12a, 2012. *Standard Terminology for Additive Manufacturing Technologies*, vol. 10.04.

Bellini, A., 2002. *Fused deposition of ceramics: A comprehensive experimental, analytical and computational study of material behaviour, fabrication process and equipment design*. Thesis (PhD). Drexel University.

Bellini, A. and Güçeri, S., 2003. Mechanical characterization of parts fabricated using fused deposition modelling. *Rapid Prototyping Journal*, 9 (4), 252–264.

Bellini, A., Shor, L., and Güçeri, S., 2005. New developments in fused deposition modelling of ceramic. *Rapid Prototyping Journal*, 11, (4), 214–220.

Boschetto, A., Giordano, V. and Veniali, F., 2013. 3D roughness profile model in fused deposition modelling. *Rapid Prototyping Journal*, 19 (4), 240–252.

Brinson, H.F. and Brinson L.C., 2008. *Polymer engineering science and viscoelasticity: an introduction*. Houston: Springer.

Brookes, K., 2014. 3D print show. *Metal Powder Report*, 69 (1), 33–35.

Céline, B., et al., 2004. Modelling of bond formation between polymer filaments in the fused deposition modelling process. *Journal of Manufacturing Processes*, 6 (2), 170–178.

Choia, J., et al., 2011. Development of a mobile fused deposition modelling system with enhanced manufacturing flexibility. *Journal of Materials Processing Technology*, 211 (3), 424–432.

Cunico, M.M., 2013. Study and optimisation of FDM process parameters for support-material-free deposition of filaments and increased layer adherence. *Virtual and Physical Prototyping*, 8, (2), 127–134.

Chua, C.K. and Leong, K.F., 2014. *3D printing and additive manufacturing: principles and applications*. London: World Scientific Publishing.

Croccolo, D., Agostinis, M., and Olmi, G., 2013. Experimental characterization and analytical modelling of the mechanical behaviour of fused deposition processed parts made of ABS-M30. *Computational Materials Science*, 79, 506–518.

Drabousky, D.P., 2009. *Prony series representation and interconversion of viscoelastic material functions of equine cortical bone*. Master thesis. Case Western Reserve University.

Espalin, D., et al., 2014. Multi-material, multi-technology FDM: exploring build process variations. *Rapid Prototyping Journal*, 20 (3), 236–244.

Galantucci, L.M., Lavecchia, F., and Percoco, G., 2009. Experimental study aiming to enhance the surface finish of fused deposition modeled parts. *CIRP Annals - Manufacturing Technology*, 58, 189–192.

Goldman Sachs, 2013. *Annual Report*. http://www.goldmansachs.com/s/2013annualreport/landing [Accessed 19 November 2014].

Gurrala, P.K, and Regalla, S.P., 2014a. Multi-objective optimisation of strength and volumetric shrinkage of FDM parts. *Virtual and Physical Prototyping*, 9 (2), 127–138.

Gurrala, P.K. and Regalla, S.P., 2014b. Part strength evolution with bonding between filaments in fused deposition modelling. *Virtual and Physical Prototyping*, 9 (3), 141–149.

Kaviany, M., 2002. *Principles of heat transfer*. New York: John Wiley & Sons.

Kothandaraman, C.P. and Subramanyan, S., 2006. *Fundamentals of heat and mass transfer*. New Delhi: New Age International.

Lee, W., Wei, C., and Chung, S., 2014. Development of a hybrid rapid prototyping system using low-cost fused deposition modeling and five-axis machining. *Journal of Materials Processing Technology*, 214 (11), 2366–2374.

Leu, M.C., et al., 2012. Freeze-form extrusion fabrication of functionally graded materials. *CIRP Annals - Manufacturing Technology*, 61 (1), 223–226.

Li, L., 2002. *Analysis and fabrication of FDM prototypes with locally controlled properties*. Thesis (PhD). University of Calgary.

Martínez, J., et al., 2013. Comparative between FEM models for FDM parts and their approach to a real mechanical behaviour. *Procedia Engineering*, 63, 878–884.

Mellor, S., Hao, L., and Zhang, D., 2014. Additive manufacturing: a framework for implementation. *International Journal of Production Economics*, 149, 194–201.

Pal, D. and Ravi, B., 2007. Rapid tooling route selection and evaluation for sand and investment casting. *Virtual and Physical Prototyping*, 2, 197–207.

Pandey, P.M., Venkata, R.N., and Dhande, S.G., 2006. Virtual hybrid-FDM system to enhance surface finish. *Virtual and Physical Prototyping*, 1, 101–116.

Pennington, R.C., Hoekstra, N.L., and Newcomer, J.L., 2005. Significant factors in the dimensional accuracy of fused deposition modelling. *Journal of Process Mechanical Engineering*, 219 (1), 89–92.

Reddy, B.V., Reddy, N.V., and Ghosh, A., 2007. Fused deposition modelling using direct extrusion. *Virtual and Physical Prototyping*, 2, 51–60.

Rezaie, R., et al., 2013. Topology optimization for fused deposition modelling process. *Procedia CIRP*, 6, 521–526.

Rodriguez, J.F., 1999. *Modelling the mechanical behaviour of fused deposition acrylonitrile-butadiene-styrene polymer components*. Thesis (PhD). University of Notre Dame.

Rodriguez, J.F., Thomas, J.P., and Renaud, J.E., 2000. Characterization of the mesostructure of fused-deposition acrylonitrile-butadiene-styrene materials. *Rapid Prototyping Journal*, 6 (3), 175–185.

Siegel, R. and Howell, J.R., 1992. *Thermal radiation heat transfer*. London: Hemisphere Publishing Corporation.

Silveira, Z.C., *et al*., 2014. Design development and functional validation of an interchangeable head based on mini screw extrusion applied in an experimental desktop 3–D printer. *International Journal of Rapid Manufacturing*, 4 (1), 49–65.

Sugavaneswaran, M. and Arumaikkannu, G., 2014. Modelling for randomly oriented multi material additive manufacturing component and its fabrication. *Materials and Design*, 54, 779–785.

Syam, W.P., Mannan, M.A., and Al-Ahmari, A.M., 2011. Rapid prototyping and rapid manufacturing in medicine and dentistry. *Virtual and Physical Prototyping*, 6, 79–109.

Thrimurthulu, K., Pandey, P.M., and Reddy, N.V., 2004. Optimum part deposition orientation in fused deposition modelling. *International Journal of Machine Tools & Manufacture*, 44 (6), 585–594.

Vogtmann, D., 2009. *Stress relaxation in PMMA during Large-Strain Compression Testing near the Glass Transition Temperature*. Thesis (PhD). Ohio University.

Wang, F., et al., 2004. Precision extruding deposition and characterization of cellular poly-caprolactone tissue scaffolds. *Rapid Prototyping Journal*, 10, (1), 42–49.

Widden, M. and Gunn, K., 2010. Design–build–test of model aerofoils for engineering education using FDM. *Virtual and Physical Prototyping*, 5, 189–194.

Yardimci, M.A., 1999. *Process analysis and planning for fused deposition*. Thesis (PhD). University of Illinois.

Yardimci, M.A. and Güçeri, S., 1996. Conceptual framework for the thermal process modelling of fused deposition. *Rapid Prototyping Journal*, 2 (2), 26–31.

Ziemian, C.W. and Crawn, P.M., 2001. Computer aided decision support for fused deposition modelling. *Rapid Prototyping Journal*, 7 (3), 138–147.